ISBN: 978-3-95450-214-1 ISSN: 2673-5490 doi:10.18429/JACoW-IPAC2021-MOPAB012

ENERGY DEPOSITION STUDY OF THE CERN HL-LHC OPTICS V1.5 IN THE ATLAS AND CMS INSERTIONS

M. Sabate-Gilarte*, F. Cerutti, CERN, Geneva, Switzerland

Abstract

The High Luminosity Large Hadron Collider (HL-LHC) is the approved CERN project aiming at further increasing the integrated luminosity of the LHC by a factor 10. As such, it implies a complete redesign of the experimental high-luminosity insertions of ATLAS and CMS. The progressive evolution of the new layout and optics requires a continuous analysis of the radiation environment, to which magnets and other equipment are exposed to. This is assured by means of Monte Carlo simulations of the collision debris on the evolving machine model. The latter featured several developments, such as the explicit inclusion of the cold protection diodes of the final focusing circuits as well as the crab cavities cryomodule.

This work presents the most updated characterization of the radiation field with FLUKA Monte Carlo simulation code and its impact in the insertion region and the dispersion suppressors of Point 1 and 5, for the HL-LHC optics v1.5 released in 2019. Various optimization and mitigation studies are highlighted, providing key information for maximizing the lifetime of new and present magnets.

INTRODUCTION

The upgrade of the LHC towards Higher Luminosity, HL-LHC [1], implies to tackle a number of complex tasks. The increase by a factor five of the levelled instantaneous luminosity up to $5{\cdot}10^{34}$ cm^{-2} s^{-1} (and $7.5{\cdot}10^{34}$ cm^{-2} s^{-1} as ultimate target) and the nominal integrated luminosity goal of 3000 fb^{-1} (4000 fb^{-1} for the ultimate scenario), represent a significant challenge for the operation of the machine. The characterization of the resulting radiation environment is one of the key aspects to be addressed. The description of particle showers induced by the collision debris and beam losses allows identifying potential weaknesses of the system and providing key design input in many respects, from heat loads on cryogenics to radiation to electronics (R2E). In particular, a careful evaluation of the energy deposition becomes crucial to prevent quenches of the superconducting magnets, estimate their lifetime or assure that the cryogenic system meets the required capacity. In this context, Monte Carlo simulations are powerful assets to describe the radiation field and FLUKA [2–4] is the reference tool at CERN for these purposes.

The experimental insertions are exposed to the most energetic components of the collision debris. They consist of a series of cold quadrupoles focusing the colliding beams, separation and recombination dipoles guiding the beams into collision, as well as corrector magnets optimizing the beam trajectory and setting up the crossing angle. This work is focused on the LHC insertions 1 and 5, hosting the ATLAS and CMS detectors, respectively, and being subject to a profound renovation for the HL-LHC upgrade.

* marta.sabate.gilarte@cern.ch

FLUKA SIMULATION DESCRIPTION

Proton-proton collisions are described in FLUKA by means of the DPMJET-3 event generator [5, 6]. Moreover, a very detailed 3D geometry has been implemented from the most updated technical drawings of the different beam line elements and tunnel structure, to produce results as accurate as possible. The positioning of the magnets and their magnetic field settings are obtained automatically thanks to the *LineBuilder* [7], which reads the optics files information.

According to the latest beam optics version, v1.5 released in May 2019, the baseline half crossing angle is 250 µrad for the two high luminosity interaction points (IP1/5). In CMS (Insertion Region 5, i.e., IR5) the beams cross in the vertical plane (VC), either with an upward or downward transverse momentum component, while in ATLAS (IR1) they cross in the horizontal plane with a transverse momentum component directed towards the external side of the ring. All the simulations presented here are normalized to nominal HL-LHC operation conditions, i.e., $5{\cdot}10^{34}$ cm^{-2}s^{-1} of instantaneous luminosity and an integrated luminosity of L_{int} = 3000 fb^{-1} for the entire HL-LHC era, with 7 TeV proton beams [1]. The adopted inelastic proton-proton cross-section, at 14 TeV centre-of-mass energy, is 85 mb as obtained by FLUKA.

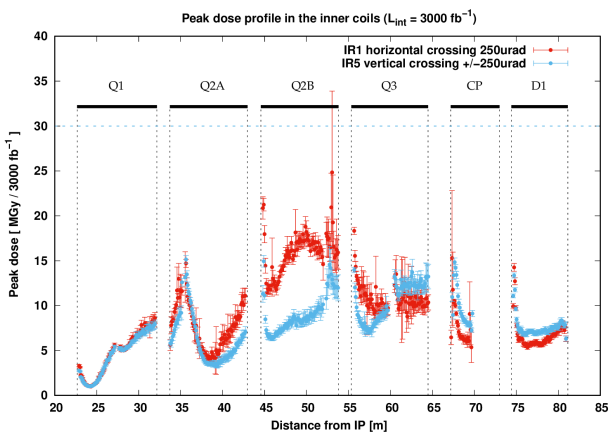

Figure 1: Peak dose profile in the inner coils of the triplet-D1 magnets for horizontal (red) and vertical (blue) crossing, assuming 250 µrad half crossing angle. In case of VC the regular polarity inversion is taken into account. The dashed line indicates the 30 MGy reference magnets lifetime limit.

This work is the continuation of previous studies [8] and accounts for the variations implied by the evolution from optics v1.3 to v1.5, in particular:

ISBN: 978-3-95450-214-1 ISSN: 2673-5490 doi:10.18429/JACoW-IPAC2021-MOPAB012

- The swap of the crossing planes between ATLAS and CMS leading to horizontal crossing (HC) in IP1 (Interaction Point 1) and vertical crossing (VC) in IP5, with the regular alternation of up and down polarities adopted as baseline in the latter case;
- The increase of the twin chamber separation in the TAXN from 148 mm (IP side) - 158 mm (non-IP side) to 151 mm - 161 mm and of the aperture from 85 mm to 88 mm (inner diameter), with the implementation of a revised TAXN model in a readjusted position;
- The update of the Corrector Package (CP) magnetic and mechanical lengths and of the interconnect (IC) design in the triplet-D1 magnet string;
- The modification of the Q4-assembly configuration, reducing the number of corrector magnets.

ENERGY DEPOSITION DUE TO COLLISION DEBRIS

Integral Heat Loads

For the nominal levelled HL-LHC luminosity of $5{\cdot}10^{34}$ cm^{-2}s^{-1}, the proton-proton collision debris carries a total power of almost 5 kW on each side of the IP. The largest fraction of the latter impacts the machine by means of the most energetic particles emitted in the very forward direction and going through the TAXS absorber aperture. If one compares the flux of particles with kinetic energy exceeding 1 GeV that enter the first quadrupole (Q1) and the one at the exit of the separation dipole (D1) being 60 m apart, it is noticeable that the reduction amounts to 90% for charged pions and kaons, between 40 and 50% for protons (except those in the 7 TeV diffractive peak), 50% for photons and 10% for neutrons. This means that the vast majority of charged mesons is captured by the traversed magnetic fields and lost in the *triplet-D1* region.

Table 1 summarises the heat loads deposited in the different magnets. The contribution on the cold masses is disentangled from the one on the beam screens, which are cooled by a separate circuit. In addition, the interconnects receive about 50 W. The variation of the crossing angle alters those values. A sensitivity study has been carried out to quantify the effect of lowering the half crossing angle from 250 µrad to 150 µrad. As a result, the total heat loads of the *triplet-D1* decrease by 2.5% for HC and 7% for VC.

Downstream, the TAXN absorber is devised to intercept the neutral particles where the vacuum chamber splits in two pipes. Their separation and aperture, together with the length of the absorbing material in between and the position of the object, determine the TAXN protection efficiency with respect to the following machine components. This is maximized for VC, with the TAXN getting 1170 W, while for HC the neutral particle cone gets closer to the outgoing beam aperture and the collected power drops to 890 W. Consequently, the recombination dipole D2 is clearly more exposed for HC, as shown in Table 1, and the aforementioned crossing angle diminution yields in this case a one third reduction in its load (which applies to the subsequent Q4 assembly too). In addition to the TAXN, the protection of the Matching Section (MS) magnets relies on a series of collimators and masks. Immediately after the TAXN and before the D2, the TCLX4 physics debris collimator is installed on the outgoing beam pipe and receives 260 W for HC and 76 W for VC. As for the Crab Cavities, the total power deposited in the cavity walls, the beam screen of the other beam and the He tank at 1.9 K is of the order of few W and less than 1 W for HC and VC, respectively. Further away along the beam line, the TCL5 receives almost 100 W and the TCL6 44 W for HC, while for VC they absorb a total power of 58 W and 39 W, respectively. Their jaws are made of a tungsten alloy, playing a critical role in minimizing the dose in the superconducting coils of the dipole correctors that are less radiation resistant than the quadrupoles. Moreover, 1 m long masks made of the same tungsten alloy in cell 4 and copper in cells 5 and 6 are planned to be installed on both beam chambers to reinforce the shielding in front of the Q4, Q5 and Q6 assemblies.

Peak Doses in the Magnet Coils

The peak dose profile in the inner coils of the *triplet-D1* magnets is shown in Fig. 1 for both crossing schemes. Thanks to the polarity alternation in VC, granting a 30% decrease of the maximum dose value, in the CMS insertion the latter does not exceed 15 MGy and is reached on the IP side of Q2A. On the other hand, in case of HC the maximum dose, in the 20 to 25 MGy range, is reached on the front face of Q2B and in the Q2B orbit corrector. Respective peak power densities, averaged over the cable radial thickness, do not surpass 2.5 mW/cm^3, remaining well below the estimated quench limit. Figure 2 illustrates the 2D transverse distribution of power density at the most exposed location, allowing to appreciate the radial gradient and the effect of the transition between different materials.

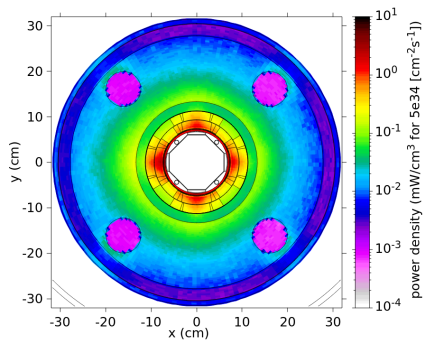

Figure 2: Power density (mW/cm^3) map in the transverse section of Q2B at the maximum location for HC.

Moving to the MS, a maximum dose of 10 MGy is reached in the D2 coils for HC, with a 15% reduction with respect to the previous v1.3 estimate [8] thanks to the optimization of the TAXN position and design. On the other hand, power densities are everywhere below 1 mW/cm^3, as provided by the protection scheme featuring collimators and masks

ISBN: 978-3-95450-214-1 ISSN: 2673-5490 doi:10.18429/JACoW-IPAC2021-MOPAB012

Table 1: Total power, in W, deposited in the *Triplet-D1* string and in the *Matching Section* magnets for $5{\cdot}10^{34}$ $cm^{-2}s^{-1}$ instantaneous luminosity and 250 µrad half crossing angle. The beam pipe extensions refer to the segments between the magnets excluding the interconnects.

	Horizontal Crossing - IR1 (ATLAS)		**Vertical Crossing - IR5 (CMS)**	
Element	**Magnet cold mass**	**Beam screen**	**Magnet cold mass**	**Beam screen**
Q1A+Q1B	110	167	114	175
Q2A+OC	98	65	101	68
Q2B+OC	134	97	123	87
Q3A+Q3B	120	69	134	80
CP-OC	46	46	65	56
D1	66	45	81	57
Beam pipe extensions	13	50	14	58
Total in the *Triplet-D1*	**587**	**539**	**632**	**581**
D2-assembly	26	2	13	1
Q4-assembly	8	1	6	1
Q5-assembly	2	0.2	3	0.2
Q6-assembly	1	<0.1	1	<0.1

behind the TAXN. The polarity alternation in VC has a sizeable effect on the Q4-assembly, where it grants a decrease of 45% in the peak dose on the IP face of the first MCBY corrector magnet. Thereby, it allows to significantly delay its replacement, if further test analysis confirm such a necessity because of an insulator radiation resistance limited to few MGy that would be exceeded before the end of the HL-LHC operation.

The same issue applies to the MCBC correctors installed in the Dispersion Suppressor (DS), where the beam line is bent by the same main dipoles of the arc. There the machine is impacted by a well defined debris component, namely the aforementioned diffractive protons with energies slightly lower than the circulating beam, which are lost in the half cells of maximum dispersion, as depicted in Fig. 3. In fact, the lattice is not exactly symmetric, with the MCBC corrector in the half cell 9 (HC9) that is closer to the IP on the left side than on the right side of the experimental cavern, since, in the outgoing beam direction, in the first case it precedes, rather than follows, the main quadrupole (Q9). Such a position exposes it much more critically to the highest loss peak in the figure, independently of the settings of the TCL6 collimator that is unable to affect the loss profile beyond the half of HC9, and consequently it is expected to reach a peak dose of 4 MGy before the end of the first HL-LHC Run (Run-4). Therefore, a replacement strategy is being prepared also for the two HC9 MCBC magnets on the left of ATLAS and CMS, envisaging the use of spare MCBY magnets whose larger aperture is compatible with the insertion of an inner shielding.

CONCLUSION

An up-to-date model of the ATLAS and CMS HL-LHC insertions has been implemented in FLUKA, incorporating the most recent layout modifications and beam optics

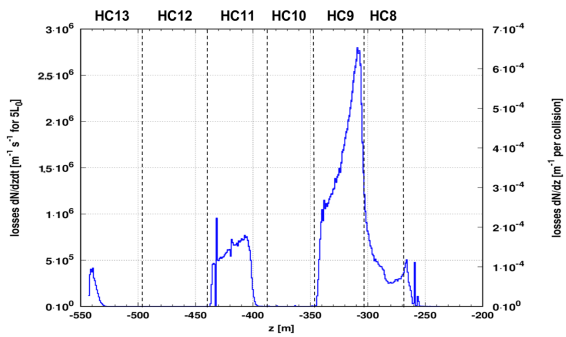

Figure 3: Proton loss distribution in the DS on the left side of IP1 (located at z=0), for the baseline TCL6 aperture of 14σ corresponding to a half gap of 2.9 mm.

such as to ensure the availability of relevant energy deposition estimates. An excerpt of new reference results has been presented in this work, focusing on integral heat loads and peak dose values in the magnet coils. These studies informed several design decisions, spanning material choices for collimator and masks, absorber optimization as well as the strategy for the foreseen replacement of certain corrector magnets in the MS and in the DS, as a function of their predicted cumulative doses.

ACKNOWLEDGEMENTS

The authors are indebted to R. De Maria (CERN), who has constantly provided the beam optics information, C. Garion, J. Hansen and their CERN team for the vacuum layout update, A. Infantino (CERN) and the HSE-RP collaborators for their joint efforts on the machine geometry model as well as to many colleagues of the HL-LHC Project - supporting this research - for their input.

ISBN: 978-3-95450-214-1 ISSN: 2673-5490 doi:10.18429/JACoW-IPAC2021-MOPAB012

REFERENCES

[1] G. Apollinari, I. Béjar Alonso, O. Brüning, P. Fessia, M. Lamont, L. Rossi, and L. Tavian, "High-Luminosity Large Hadron Collider (HL-LHC): Technical Design Report", CERN, Geneva, Switzerland, Rep. CERN-2020-010, 2020, doi:10.23731/CYRM-2020-0010

[2] FLUKA, https://fluka.cern

[3] G. Battistoni *et al.*, "Overview of the FLUKA code", *Annals of Nuclear Energy*, vol. 82, pp. 10-18, 2014. doi:10.1016/j.anucene.2014.11.007

[4] T. T. Bohlen *et al.*, "The FLUKA Code: Developments and Challenges for High Energy and Medical Applications", *Nuclear Data Sheets*, vol. 120, pp. 211-214, 2014. doi:10.1016/j.nds.2014.07.049

[5] S. Roesler, R. Engel, and J. Ranft, "The Monte Carlo Event Generator DPMJET-III", in *Proc. Monte Carlo 2000 Conference*, Lisbon, Oct. 2000. doi:10.2172/784800

[6] A. Fedynitch, "Cascade equations and hadronic interactions at very high energies" PhD Thesis, KIT, Karlsruhe, Germany, Nov. 2015, https://cds.cern.ch/record/2231593/files/CERN-THESIS-2015-371.pdf

[7] A. Mereghetti *et al.*, "The FLUKA linebuilder and element database: tools for building complex models of accelerator beam lines", in *Proc. IPAC'12*, New Orleans, LA, USA, May 2012, paper WEPPD071, pp. 2687-2689.

[8] A. Tsinganis and F. Cerutti, "Impact of collision debris in the HL-LHC ATLAS and CMS insertions", in *Proc. IPAC'17*, Copenhagen, Denmark, May 2017. paper TUPVA021.